

## Article

# Epoxidation of Fatty Acid Methyl Esters with Hydrogen Peroxide Catalyzed by Peroxopolyoxotungstate PW4 Encapsulated in the MIL-100(Cr) Framework

Anton L. Esipovich<sup>1,2</sup>, Evgeny A. Kanakov<sup>1,2,\*</sup> , Tatyana A. Charykova<sup>1,2</sup> and Ksenia V. Otopkova<sup>1,2</sup>

<sup>1</sup> Dzerzhinsk Polytechnic Institute, Engineering and Technology Faculty, Nizhny Novgorod State Technical University n.a. R.E. Alekseev, 603950 Nizhny Novgorod, Russia

<sup>2</sup> Chemistry Department, Lobachevsky State University of Nizhny Novgorod, 603950 Nizhny Novgorod, Russia

\* Correspondence: kan-evg@mail.ru

**Abstract:** The MIL-100(Cr), PW12@MIL-100(Cr) and PW4@MIL-100(Cr) catalysts were prepared and characterized through XRD, FTIR, BET, SEM, EDS and Raman spectroscopy. A comparison of the catalytic properties of the synthesized materials in the epoxidation of FAMES with hydrogen peroxide was made. The PW4@MIL-100(Cr) catalyst exhibited the highest catalytic activity and provided a high selectivity for the formation of epoxides. The effects of the reaction temperature, catalyst loading, reaction time and FAME:hydrogen peroxide molar ratio on the reaction performance were investigated, and the optimal process conditions were determined. An epoxide yield of 73% with a selectivity of 77% could be obtained using PW4@MIL-100(Cr) after 4 h at 40 °C. The catalytic stability test showed that PW4@MIL-100(Cr) could be easily separated and reused without any treatment for at least five consecutive cycles without a loss of activity or selectivity.

**Keywords:** fatty acid methyl esters; metal–organic frameworks; epoxidation; polyoxotungstates; phosphotungstic acid; MIL-100(Cr)



**Citation:** Esipovich, A.L.; Kanakov, E.A.; Charykova, T.A.; Otopkova, K.V. Epoxidation of Fatty Acid Methyl Esters with Hydrogen Peroxide Catalyzed by Peroxopolyoxotungstate PW4 Encapsulated in the MIL-100(Cr) Framework. *Catalysts* **2023**, *13*, 138. <https://doi.org/10.3390/catal13010138>

Academic Editors: Arindam Modak, Kamal Kishore Pant and Asim Bhaumik

Received: 8 December 2022

Revised: 30 December 2022

Accepted: 3 January 2023

Published: 6 January 2023



**Copyright:** © 2023 by the authors. Licensee MDPI, Basel, Switzerland. This article is an open access article distributed under the terms and conditions of the Creative Commons Attribution (CC BY) license (<https://creativecommons.org/licenses/by/4.0/>).

## 1. Introduction

Fatty acid methyl esters (FAMES), which are currently used as fuels, are promising raw materials for the production of a wide range of organic substances, e.g., corrosion inhibitors, surfactants, biolubricants, etc. [1–6].

A promising route of FAME utilization is the production of polyvinyl chloride (PVC) stabilizers and plasticizers. These products are currently produced in industry by a homogeneous catalytic conventional epoxidation of vegetable oils and fatty acid esters (FAEs). Performic acid and peracetic acid, which are formed in situ from hydrogen peroxide and corresponding carboxylic acid, are mainly used as oxidants. The main disadvantages of the conventional technology are the corrosion problems caused by the strong acids in an oxidizing environment, its instability and the explosiveness of peracids as well as their high reactivity, which leads to the formation of a large number of byproducts.

The use of hydrogen peroxide (H<sub>2</sub>O<sub>2</sub>) as an oxidant in combination with heterogeneous catalysts eliminates these problems. Hydrogen peroxide is one of the most powerful available oxidizing agents. At the same time, hydrogen peroxide aqueous solutions are safe for storage, operation and transportation. Moreover, hydrogen peroxide is a commercially available, inexpensive and relatively nontoxic reagent [7–12].

Nowadays, titanium silicates are the most effective systems for the heterogeneous liquid-phase oxidation of various organic substrates with H<sub>2</sub>O<sub>2</sub> [13]. Among these catalytic systems, a special place is occupied by the microporous TS-1 catalyst, which is considered to be the best oxidation catalyst. Titanium silicate TS-1 exhibits a high catalytic activity in the oxidation of various organic substances with hydrogen peroxide, e.g., the hydroxylation of arenes, the oxidation of n-hydrocarbons, the epoxidation of olefins, the

oxidation of thioethers, the ammoximation of ketones and a number of other important processes [14–19].

Recent studies have demonstrated the use of micro- and mesoporous TS-1 as a heterogeneous catalyst in liquid-phase FAME epoxidation with  $H_2O_2$  [20,21]. A conversion of methyl oleate of 93% and a selectivity for 9,10-epoxy methyl stearate of 87% were attained after 24 h at 50 °C in acetonitrile. Amorphous xerogel  $TiO_x-SiO_2$  and mesoporous titanium silicate Ti-MCM-41 were less effective.

The major drawback of the microporous titanium silicates is the small size of their pores (5.3–5.6 Å), which makes it difficult to use these catalysts in reactions with large molecules (for example, triglycerides, FAMEs, cyclic compounds, etc.). It was found that micro- and mesoporous titanium silicates are rapidly deactivated by blocking their active Ti-sites with organic deposits, which are presumably formed by the consecutive reactions of their target products, such as dimerization or oligomerization [22,23].

Alternatively, organic hydroperoxides (typically, tert-butyl hydroperoxide, TBHP, or cumyl hydroperoxide, CHP) can be used as oxidizing agents. Corma and coworkers tested the epoxidation with both  $H_2O_2$  and TBHP of methyl oleate using titanium-containing beta zeolite (Ti-BEA) and Ti-MCM-41 materials (Ti-MCM41) [24]. With hydrogen peroxide in acetonitrile, Ti-BEA showed better yields than Ti-MCM-41 (44% vs. 24%). At same time, with TBHP, the epoxide yields over Ti-BEA and Ti-MCM-41 were 48% vs. 59%, respectively.

High yields (>98%) for the mono- and diepoxide derivatives of FAMEs were obtained using Ti-MCM-41 with TBHP as an oxidant [25]. The process was carried out in ethyl acetate solution for 24 h at a temperature of 90 °C.

An epoxide yield of about 20% was achieved with a selectivity close to 90% in toluene solution for 25 h at 70 °C using a Ti-SiO<sub>2</sub> catalyst [26]. The reusability of the catalyst was evaluated with four experiments with the same catalyst, which was filtrated after every experiment. It was shown that the catalyst was reusable at least four times without significant drop-in activity [27].

Despite the fact that titanium-containing catalysts exhibited a greater stability when TBHP was used as an oxidant, the use of hydrogen peroxide seems to be preferable. The FAME epoxidation process was carried out at elevated temperatures when TBHP was used, and alcohol was formed as a byproduct. In addition, TBHP is much more expensive [27].

Polyoxometalates (POMs) and peroxopolyoxometalates (PPOMs) are promising catalysts for selective liquid-phase oxidation. Such systems attract attention with the wide possibilities of their use in various fields of organic chemistry [28,29]. Tungsten-based POMs are used as catalysts for the epoxidation of various alkenes with hydrogen peroxide. Venturello's [30] and Ishii's [31] groups investigated the selective epoxidation of nonpolar olefins in biphasic reaction media using the  $[PO_4\{W(O)(O_2)_2\}_4]^{3-}$  PPOM catalyst. Poli et al. [32] studied the epoxidation of FAMEs in the presence of a tungsten-containing catalyst called "Tetrakis" ( $[(C_8H_{17})_3NCH_3]^{3+} [PO_4\{W(O)(O_2)_2\}_4]^{3-}$ ). A conversion of substrates of 90–95% and a selectivity for epoxides of 85–90% were achieved.

Despite the high activity of POM-based catalysts in the oxidation and epoxidation of large organic substrates, these catalytic systems were soluble in the reaction media, which necessitated a difficult stage of their separation.

To solve this problem, the use of immobilized POMs was proposed. Silicate [33,34] ion-exchange resins [35,36], various polymeric materials modified with ionic liquids [37], are used as supports for the heterogenization of POMs in the scientific literature. However, several drawbacks are associated with these materials, including the low loading of POMs, their leaching, the conglomeration of their particles, etc.

Recently, metal–organic frameworks (MOFs) have attracted increasing attention due to their unique structures and wide applications in various fields, such as gas adsorption/separation, catalysis, sensors, drug delivery, magnetic materials, optical devices, etc. [37–42].

MOFs are an excellent material for the support of various catalysts due to their porous structure and high stability [38,43–45]. Polyoxotungstates  $[PW_4O_{24}]^{3-}$  (PW4) and

[PW<sub>12</sub>O<sub>40</sub>]<sup>3-</sup> (PW12) can be inserted into the nanocages of the metal organic framework MIL-101 [33]. These catalysts were tested in the selective epoxidation of alkenes (3-carene, limonene, R-pinene, cyclohexene, cyclooctene and 1-octene). The hybrid PW4/MIL-101 and PW12/MIL-101 materials demonstrated similar catalytic activities in H<sub>2</sub>O<sub>2</sub>-based alkene epoxidation, which was comparable to the activity of the corresponding homogeneous PW<sub>x</sub>. Both materials behaved as true heterogeneous catalysts and could be recycled several times (4–5 cycles). However, some deterioration of the catalytic properties occurred after several reuses because of the partial destruction of the MIL-101 matrix and/or the filling of the pores with the reaction products [46].

Moreover, the phosphotungstic acid (PTA) molecules would leach out during the epoxidation process due to their size (10.0 Å) being smaller than the window size of MIL-101 (16.0 × 16.0 Å<sup>2</sup>), which led to a decrease in the catalyst activity in the recycled runs. If the size of the POMs was smaller than that of the nanocages but larger than the window size of the MOFs, the POMs could be confined in the pores of the MOFs to prevent leaching. However, the catalytic performance might decrease with the narrowing of the windows of the MOFs due to the slower mass transfer [47].

MIL-100 is a carboxylate porous MOF with two types of mesopore cages of free apertures of ca. 25.0 Å and 29.0 Å that are accessible through microporous windows of ca. 5.8 × 5.8 Å<sup>2</sup> and 8.6 × 8.6 Å<sup>2</sup>. Thus, the geometry of MIL-100 should prevent the leaching of the encapsulated PTA.

A bifunctional catalyst based on MIL-100(Cr) was used for selective sorbitol production from cellulose [48]. Phosphotungstic acid was encapsulated into the MOF structure followed by modifying the resulting composite with RuCl<sub>3</sub>. This catalyst allowed the achievement of high yields of sorbitol of up to 95.1%.

The authors [49] studied the hydroxylation of phenol with formaldehyde to bisphenol F in the presence of phosphotungstic acid and immobilized on metal–organic frameworks MIL-100 (Fe or Cr) and MIL-101 (Fe or Cr). The results showed that catalysts based on MIL-100 had a higher catalytic activity compared to those based on MIL-101. Moreover, PTA/MIL-100(Fe) retained its catalytic activity for at least six cycles.

The present work considered the use of hybrid materials based on polyoxotungstates PW4 and PW12 encapsulated in the metal–organic framework MIL-100(Cr) for the FAME epoxidation process. The catalysts were synthesized and characterized through elemental analysis, SEM, XRD, N<sub>2</sub> adsorption, Raman spectroscopic studies and FTIR. The catalytic activity, selectivity and stability of the obtained catalysts were studied during the epoxidation of the FAMEs of rapeseed oil with hydrogen peroxide in acetonitrile.

## 2. Results and Discussion

### 2.1. Catalyst Characterization

The MIL-100(Cr), PW12@MIL-100(Cr) and PW4@MIL-100(Cr) catalysts were prepared and characterized through XRD, FTIR, BET, SEM, EDS and Raman spectroscopy. MIL-100(Cr) and PW12@MIL-100(Cr) were obtained through the hydrothermal method (see Sections 3.2.1 and 3.2.2). PW4@MIL-100(Cr) was obtained by treating PW12@MIL-100(Cr) with hydrogen peroxide and phosphoric acid (see Section 3.2.3).

The obtained catalyst powders had irregular morphologies with particle sizes ranging from several hundred nanometers to several micrometers (see Supplementary Materials, Figures S1–S3). The obtained MIL-100(Cr) sample consisted of clusters with rough surfaces formed by nanoparticles with a size of 50–250 nm, which was consistent with the data obtained earlier [50]. At the same time, PW4@MIL-100(Cr) and PW12@MIL-100(Cr) were characterized by the presence of larger particles (2–10 μm) formed due to the agglomeration of smaller particles.

The BET surface area (Table 1, Supplementary Materials Figures S6–S10) of PW12@MIL-100(Cr) was 409 m<sup>2</sup>·g<sup>-1</sup>, which was remarkably low compared with that of MIL-100(Cr) (1383 m<sup>2</sup>·g<sup>-1</sup>). After the PW12@MIL-100(Cr) treatment with hydrogen peroxide, the surface area of the obtained PW4@MIL-100(Cr) sample increased to 910 m<sup>2</sup>·g<sup>-1</sup>. This was due to

the leaching of the excess PTA from the surface, which was also confirmed through an EDS analysis (Table 2).

**Table 1.** Catalyst textural properties.

Catalyst	BET Surface Area ( $\text{m}^2 \cdot \text{g}^{-1}$ )	Pore Volume ( $\text{cm}^3 \cdot \text{g}^{-1}$ )	Brønsted Acid Center Concentration ( $\text{mmol} \cdot \text{g}^{-1}$ )
MIL-100(Cr)	$1383 \pm 32$	1.1	0.9
PW12@MIL-100(Cr)	$409 \pm 9$	0.3	2.7
PW4@MIL-100(Cr)	$910 \pm 26$	0.5	1.7

**Table 2.** Catalyst EDS analysis results.

Catalyst	C (atomic%)	Cr (atomic%)	P (atomic%)	W (atomic%)	P/W/Cr Ratio
MIL-100(Cr)	58.16	5.63	-	-	-
PW12@MIL-100(Cr)	48.98	4.95	0.58	7.02	1/12.1/8.5
PW4@MIL-100(Cr)	54.21	4.98	0.46	2.13	1/4.6/10.8

The EDS mapping indicated that the samples were uniform and that the elements were well distributed (see Supplementary Materials, Figures S4 and S5).

The XRD patterns of the prepared materials (Figure 1b–d) confirmed the formation of the MIL-100(Cr) structure and its retention in the phosphotungstate-containing samples by comparison with the MIL-100(Cr) simulated pattern from the crystal structure data [51] (Figure 1a). For the simulation of the MIL-100(Cr) patterns, XRD was performed using Vesta software (K. Momma and F. Izumi) “VESTA 3” for the three-dimensional visualization of the crystal, volumetric and morphology data [52].

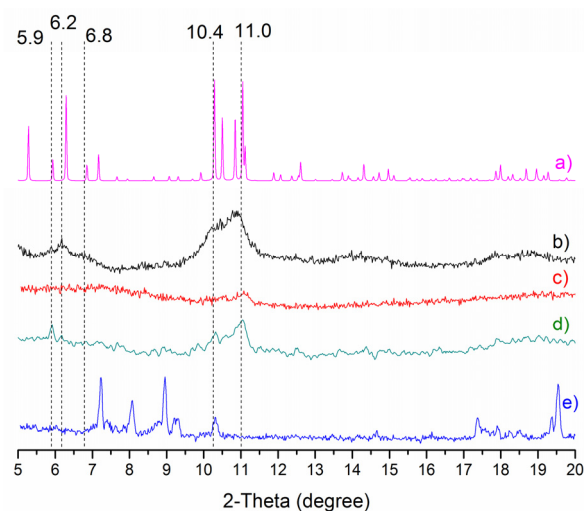


**Figure 1.** XRD patterns of simulated MIL-100(Cr) (a), MIL-100(Cr) (b), PW12@MIL-100(Cr) (c), PW4@MIL-100(Cr) (d) and PTA (e).

The MIL-100(Cr) sample (Figure 1b) had peaks of about  $5.9^\circ$ ,  $6.2^\circ$ ,  $6.8^\circ$ ,  $10.4^\circ$  and  $11.0^\circ$  angles corresponding to the MIL-100(Cr) structure reported in the literature [53].

For the PW12@MIL-100(Cr) sample, only peaks for angles of  $10.4^\circ$  and  $11.0^\circ$  were observed in the XRD pattern (Figure 1c). The differences in the relative intensities of the peaks in the MIL-100(Cr) pattern compared to those in the patterns of the PW12@MIL-100(Cr) sample could be accounted for by the high loading of PTA, which was highly dispersed on the support surface as noncrystalline species [49,54].

The intensity of the peaks in the PW4@MIL-100(Cr) diffraction pattern was higher ( $5.9^\circ$ ,  $6.2^\circ$ ,  $10.4^\circ$  and  $11.0^\circ$ ) compared with that of the PW12@MIL-100(Cr) diffraction pattern, which was also related to the leaching of the excess PTA.

It should be noted that there were no peaks which corresponded to PTA in the diffraction patterns of the phosphotungstate-containing samples (Figure 1c–e). This indicated a good distribution of POMs and PPOMs throughout the volume of the obtained composite materials [49].

The FTIR spectra of the prepared materials showed all the vibrational bands characteristic of the framework-coordinated carboxylate groups expected in the MIL-100(Cr) structure (Figure 2a–c). The bands at around  $1388$  and  $1458\text{ cm}^{-1}$  (Figure 2a) were assigned to the coordination of the tricarboxylate [53,55], and the multiple absorption peaks at  $1500$ – $1750\text{ cm}^{-1}$  were assigned to the characteristic absorption peaks of the benzene rings. The bands at  $524\text{ cm}^{-1}$  could be assigned to the Cr–O bonds of the MOF compound [50]. Thus, the FTIR analysis also confirmed the retention of the MIL-100(Cr) structure after the preparation of the phosphotungstate-containing samples PW12@MIL-100(Cr) and PW4@MIL-100(Cr).

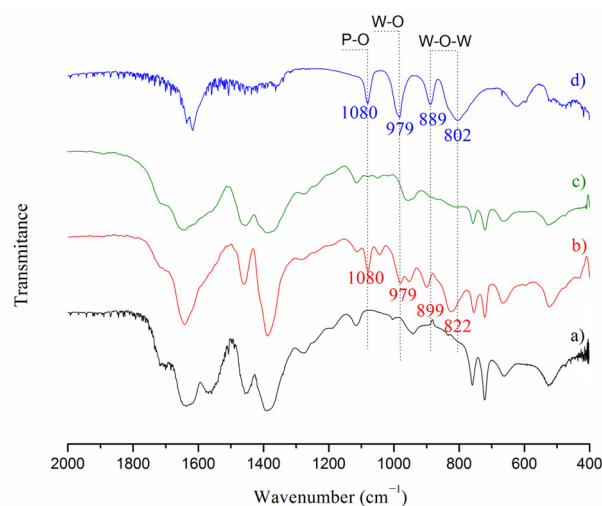


**Figure 2.** FTIR spectra of MIL-100(Cr) (a), PW12@MIL-100(Cr) (b), PW4@MIL-100(Cr) (c) and PTA (d).

The FTIR spectrum of PW12@MIL-100(Cr) (Figure 2b) had bands specific to PTA:  $1080$  (vibrational frequency of P–O<sub>a</sub>),  $979$  (stretching of W=O<sub>d</sub>),  $899$  (vibrational frequency of W–O<sub>b</sub>–W) and  $822\text{ cm}^{-1}$  (W–O<sub>c</sub>–W vibration), where a, b, c and d designated the specific positions of the oxygen atoms in the Keggin structure, namely P–O<sub>a</sub>–W<sub>3</sub>, O<sub>d</sub>=W, W–O<sub>b</sub>–W and W–O<sub>c</sub>–W, connecting two W<sub>3</sub>O<sub>13</sub> units through corner sharing and edge sharing, respectively [56]. The characteristic peaks of pure phosphoric tungsten acid ( $889$  and  $802\text{ cm}^{-1}$ ) were shifted to  $899$  and  $822\text{ cm}^{-1}$ , which indicated the inclusion of PTA in the support structure [49].

Since the bands corresponding to PW4 (Figure 2c) were rather weak due to the lower FTIR sensitivity [46], Raman spectroscopy was used to characterize this material (Figure 3).

The typical Raman spectrum of MIL-100(Cr) was obtained with peaks at around  $820$  and  $1000\text{ cm}^{-1}$ , which was identical to those of the reported data in the literature (Figure 3a) [57,58].

The PW12@MIL-100(Cr) spectrum (Figure 3b) showed an intense peak at  $1000\text{ cm}^{-1}$ . This peak corresponded to the W=O stretch in PTA [59]. At same time, the Raman spectrum of PW4@MIL-100(Cr) (Figure 3c) showed a slight shift of this peak to  $956\text{ cm}^{-1}$  and had additional peaks at  $876$  (vibrational frequency of O–O),  $636$  (vibrational frequency of W–O–O<sub>asym</sub>),  $565$  (vibrational frequency of W–O–O<sub>sym</sub>) and  $323\text{ cm}^{-1}$  (vibrational frequency of W–OH<sub>2</sub>), which confirmed the PW4 formation [60].

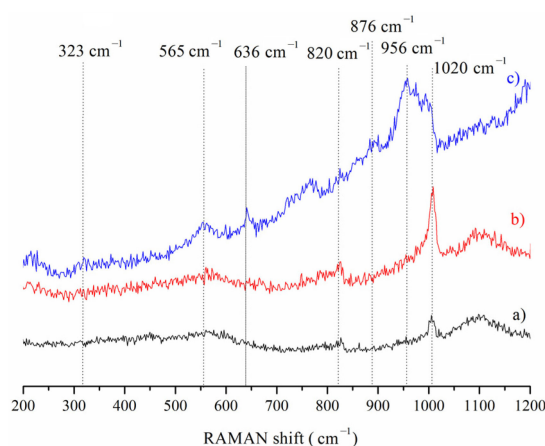


**Figure 3.** Raman spectra of MIL-100(Cr) (a), PW12@MIL-100(Cr) (b) and PW4@MIL-100(Cr) (c).

The PW4@MIL-100(Cr) formation was also confirmed by the results of the elemental analysis (Table 1). For the sample PW12@MIL-100(Cr), the P/W molar ratio was 12.10. After the hydrogen peroxide treatment, the P/W molar ratio decreased to 4.60. It was connected to the predominant PW12 transformation into PW4.

## 2.2. Catalytic Epoxidation

The catalytic performance of MIL-100(Cr), PW12@MIL-100(Cr) and PW4@MIL-100(Cr) was assessed during rapeseed FAME epoxidation with aqueous H<sub>2</sub>O<sub>2</sub> in an acetonitrile medium. Acetonitrile was chosen as the solvent in order to minimize the acid-catalyzed side reactions of the FAME epoxide.

The identification of FAME epoxidation products was performed through GC-MS. In all cases, the major products were FAME epoxides and oxidative cleavage products (nonanal, methyl 9-oxononanoate, etc.). In addition to the main products, some ketones (9-oxostearate, methyl 10-oxostearate, etc.) were found in the reaction medium (see Supplementary Materials, Figure S11).

It should also be noted that epoxide hydrolysis products (diols) were not detected in any case. Diols were detected with the additional introduction of 0.1 N hydrochloric acid into the reaction mixture. Apparently, diols are quickly consumed with the formation of oligomerization products in the presence of epoxides.

Oligomerization products were also detected through HPLC-MS chromatography. The molecular masses of the detected ions were in the range of 500–900 Da (see Supplementary Materials, Figure S12).

Methyl stearate and the preprepared epoxides of FAMEs were used as substrates to determine the byproduct formation route. Oxidation was carried out in acetonitrile in the presence of PW4@MIL-100(Cr) at 60 °C for 4 h (substrate content of 1 wt%, molar ratio of substrate:H<sub>2</sub>O<sub>2</sub> of 1:8 and catalyst content of 15 g·L<sup>-1</sup>).

The epoxide conversion was 81% after 4 h during the oxidation of FAME epoxides with hydrogen peroxide. Nonanal and methyl 9-oxononanoate (total yield of 12.2%), formed through oxidative cleavage, as well as methyl 9-oxostearate and methyl 10-oxostearate (total yield of 3.5%), formed through rearrangement, were detected as the main products.

When methyl stearate was used as a substrate, its conversion was about 50% after 4 h. Methyl oxostearates, formed through the oxidation of the carbon skeleton at various positions, were detected as the main products (see Supplementary Materials, Figure S13).

Thus, the reactions occurring during the epoxidation of FAMEs with hydrogen peroxide are presented in the scheme shown in Figure 4.

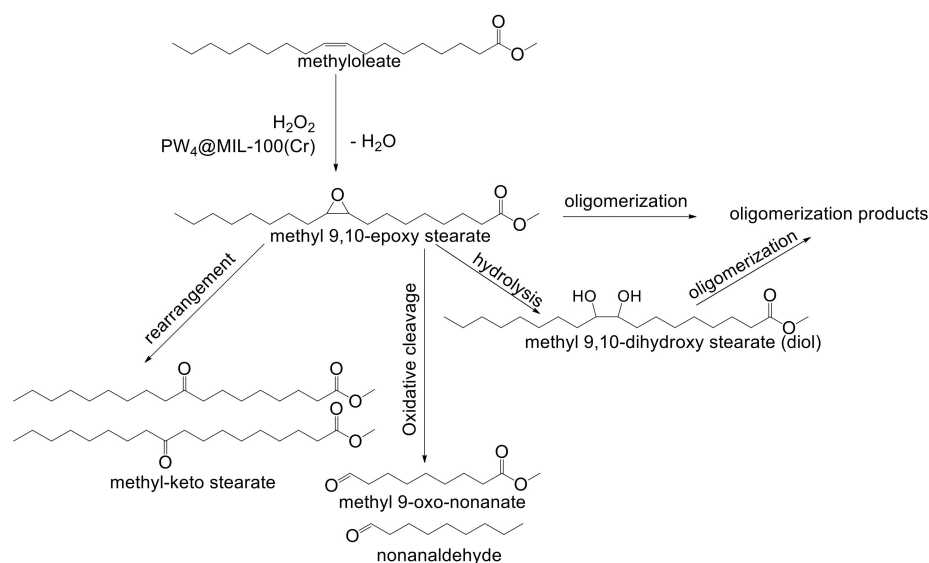


**Figure 4.** The proposed scheme of the reactions occurring during the epoxidation of FAMES.

Table 3 presents the results of the catalytic tests of MIL-100(Cr), PW12@MIL-100(Cr) and PW4@MIL-100(Cr).

**Table 3.** Catalytic tests of MIL-100(Cr), PW12@MIL-100(Cr) and PW4@MIL-100(Cr) <sup>a</sup>.

Catalyst	T, °C	Unsaturated FAME Conversion (%)		Hydrogen Peroxide Conversion (%)		Selectivity (%)							
						FAME Epoxides		Nonanal, Methyl 9-Oxononanoate		Oxostearates		Others	
		1	4	1	4	1	4	1	4	1	4	1	4
none	50	>1	1	3	8	-	-	62	62	-	-	38	38
	70	10	23	9	29	10	19	5	14	6	5	78	60
MIL-100(Cr)	50	7	18	36	64	17	22	45	28	13	5	26	46
	70	28	44	49	86	21	22	20	16	2	2	57	61
PW12@MIL-100(Cr)	50	5	24	7	31	33	24	25	17	6	4	36	55
	70	23	59	48	84	14	12	16	15	2	2	68	71
PW4@MIL-100(Cr)	50	69	98	38	81	76	49	8	15	2	3	14	33
	70	100	100	87	99	36	22	11	14	3	4	50	60

<sup>a</sup> FAME content of 1 wt%, molar ratio of unsaturated FAMES:H<sub>2</sub>O<sub>2</sub> of 1:8 and catalyst content of 15 g·L<sup>-1</sup>.

The FAME conversion without a catalyst was negligible at 50 °C and reached only 22.7% at an epoxide selectivity of 19.4% after 4 h and after increasing the temperature to 70 °C. High-molecular-weight compounds as main products (selectivity of more than 60%) were forming in the reaction mixture as a result of oxidative condensation.

The FAME consumption rate increased in the presence of MIL-100(Cr). It is known that coordinatively unsaturated metal sites (CUS) can be easily generated in the structure of MILs and that they exhibit a sufficiently high activity for certain oxidation processes, such as sulfoxidation with H<sub>2</sub>O<sub>2</sub> [61], the oxidation of cyclohexane [62], hydrocarbon oxidation [63], etc.

It should be noted that the selectivity for epoxides (21.8%) and byproducts in the presence of MIL-100(Cr) did not change significantly compared to the noncatalytic process. However, the degree of the inappropriate consumption of hydrogen peroxide increased significantly due to the sufficiently high acidity of the MOF. Brønsted acidity was present in MIL-100(Cr), resulting from both the Cr-OH groups and coordinated water due to a cooperative effect of the cation on the coordinated water molecule [64]. The determined concentration of the MIL-100(Cr) Brønsted acid centers was 0.9 mmol·g<sup>-1</sup> (Table 1). More-

over, the CUS chromium(III) centers could provide accessible sites for guest molecules, therefore playing the role of Lewis acid sites [64].

The PW4 incorporated within the MIL-100(Cr) matrix showed a fairly good catalytic activity and selectivity. The reaction over PW4@MIL-100(Cr) gave an epoxide with a 76% selectivity at a 69% substrate conversion at 50 °C after 1 h of reaction.

At the same time, the PW12@MIL-100(Cr) sample was significantly less active and showed results similar to the MIL-100(Cr) results. Only with an increase in the temperature and the time of the process were differences in the catalytic activity observed, which could be explained by the in situ conversion of PW12 to PW4 and other peroxotungstates.

### 2.2.1. Patterns of FAME Epoxidation with Hydrogen Peroxide Using the PW4@MIL-100(Cr) Catalyst

The detailed data on the byproduct yields depending on the reaction condition are presented in Table 4.

**Table 4.** The yields of the FAME epoxidation products.

Catalyst Content (g·L <sup>-1</sup> )	Unsaturated FAME:H <sub>2</sub> O <sub>2</sub> Molar Ratio	T, °C	Yield (%)							
			FAMEs Epoxides		Nonanal, Methyl 9-Oxononate		Oxostearates		Others	
			Time, h							
			1	4	1	4	1	4	1	4
15	1:8	30	23	67	2	3	0	1	1	7
15	1:8	40	43	73	2	7	1	1	3	14
15	1:8	50	53	48	6	14	1	3	10	33
15	1:8	60	67	24	8	12	2	4	21	60
15	1:8	70	36	22	11	14	3	4	50	60
30	1:8	60	42	7	12	15	3	5	41	72
7.5	1:8	60	62	36	6	9	1	3	14	52
3.75	1:8	60	46	59	5	11	1	2	9	24
15	1:4	60	65	48	7	11	1	2	18	37
15	1:2	60	64	53	4	5	1	1	12	25
15	1:2	40	29	62	2	5	1	1	5	8
15	1:1	40	47	39	3	3	1	1	10	19

Figure 5 shows the dependence of the unsaturated FAME conversion and the epoxide selectivity on the reaction temperature in the presence of the PW4@MIL-100(Cr) catalyst.

With an increase in the reaction time, a decrease in the epoxide selectivity was observed in all cases due to the sequential reactions of their cleavage and oligomerization. The decrease in the epoxide selectivity was lower at low temperatures.

The highest epoxide yield (73.5%) was achieved at 40 °C after 4 h. The rate of unsaturated FAME consumption increased sharply at higher temperatures. However, the epoxide formation selectivity was significantly reduced, and the rate of hydrogen peroxide decomposition was increased. In addition, significant consumption of methyl palmitate and methyl stearate was observed with ketone formation at 60 °C and higher temperatures. The conversion of saturated FAMEs was about 20.0% at 60 °C after 4 h.

The catalyst loading had a significant effect on the epoxidation reaction (Figure 6).

The highest epoxide yield (70%) at 60 °C and a molar ratio of unsaturated FAMEs:H<sub>2</sub>O<sub>2</sub> of 1:8 was achieved after 45 min when the PW4@MIL-100(Cr) catalyst loading was 15 g·L<sup>-1</sup>.

Increasing the catalyst loading to 15 g·L<sup>-1</sup> did not lead to a significant increase in the FAME conversion. However, the epoxide yield was significantly reduced due to the side reactions. The yield of the epoxidized FAMEs did not exceed 65% with a decrease in the catalyst loading due to the increase in the reaction time, which was necessary to achieve

high ester conversions, as a result of which the resulting epoxides were consumed by the side reactions.

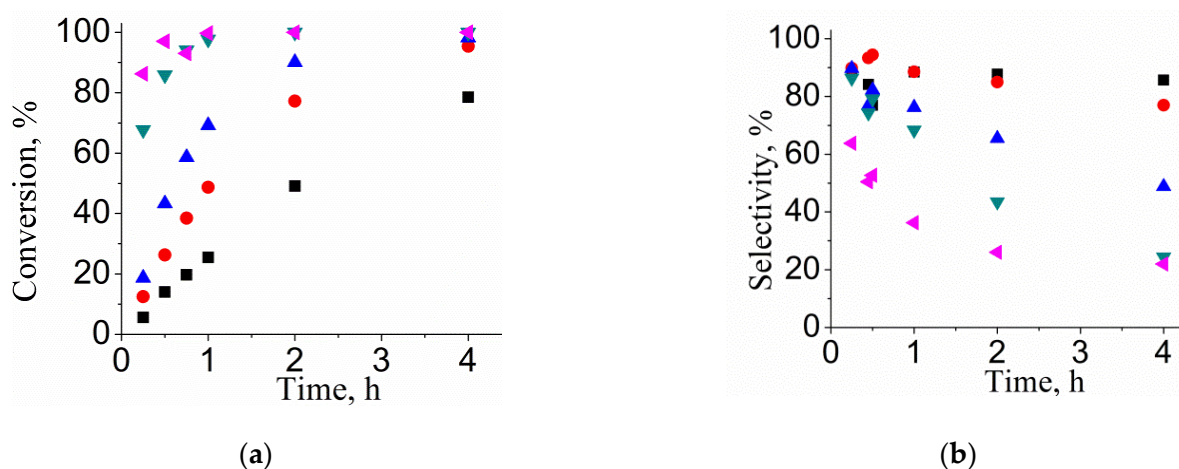


**Figure 5.** The temperature influence on the FAME conversion (a) and epoxide selectivity (b). Reaction conditions: FAME content of 1 wt%; catalyst content of 15 g·L<sup>-1</sup>; unsaturated FAME:H<sub>2</sub>O<sub>2</sub> molar ratio of 1:8; and temperature of 30 °C (■), 40 °C (●), 50 °C (▲), 60 °C (▼) and 70 °C (◀).

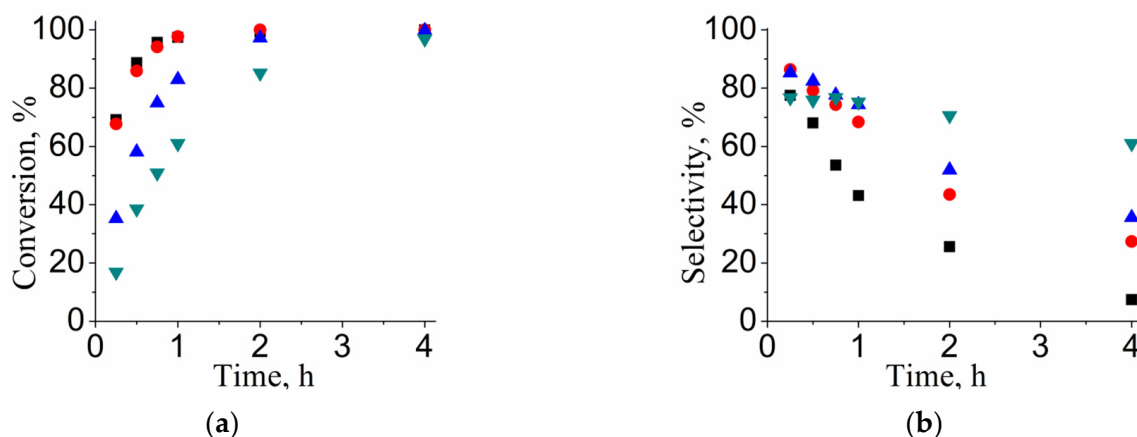


**Figure 6.** The catalyst loading influence on the unsaturated FAME conversion (a) and epoxides selectivity (b). Reaction conditions: FAME content of 1 wt%; unsaturated FAME:H<sub>2</sub>O<sub>2</sub> molar ratio of 1:8; temperature of 60 °C; and catalyst loading of 30 g·L<sup>-1</sup> (■), 15 g·L<sup>-1</sup> (●), 7.5 g·L<sup>-1</sup> (▲) and 3.75 g·L<sup>-1</sup> (▼).

The molar ratio of unsaturated FAMES:hydrogen peroxide did not significantly affect the epoxide selectivity (Figure 7) at the initial reaction stages (15–60 min). An increase in the excess hydrogen peroxide with a longer reaction time led to a sharp decrease in the epoxide yield due to the epoxide conversion side reactions. The maximum epoxidized FAME yield (~70%) after 45 min was observed with a molar ratio of FAMES:hydrogen peroxide of 1:8 at 60 °C and a catalyst content of 15 g·L<sup>-1</sup>.

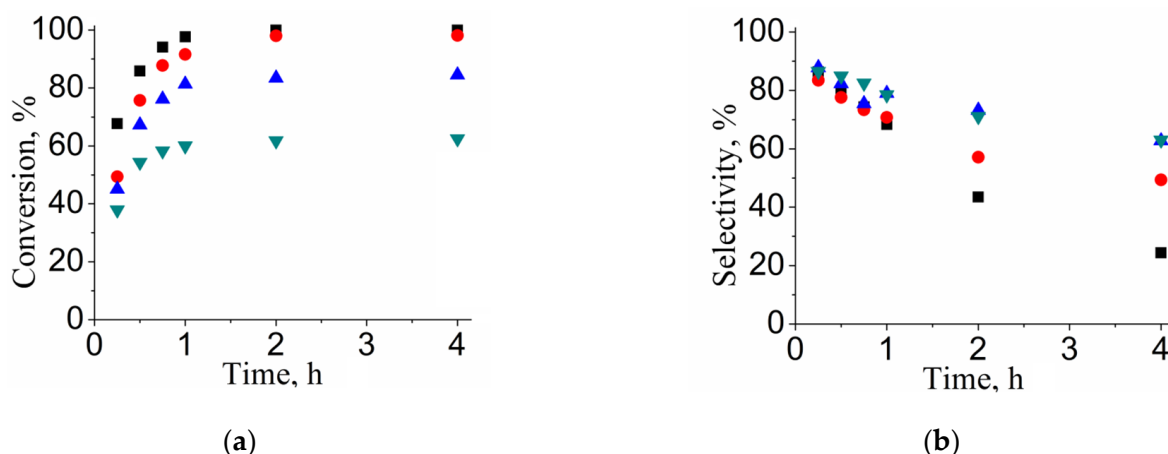


**Figure 7.** The unsaturated FAME:hydrogen peroxide molar ratio influence on the unsaturated FAME conversion (a) and epoxide selectivity (b). Reaction conditions: FAME content of 1 wt%; temperature of 60 °C, catalyst loading of 15 g·L<sup>-1</sup>; and unsaturated FAME:H<sub>2</sub>O<sub>2</sub> molar ratio of 1:8 (■), 1:4 (●), 1:2 (▲) and 1:1 (▼).

### 2.2.2. Catalyst Stability and Recycling

The test for leaching was carried out according to the recommendations of Sheldon [65]. The catalyst was filtered from the reaction media at the reaction temperature to avoid the readsorption of the leached materials, and the filtrate was allowed to react further. After the removal of the catalyst, only about 3% of further FAME conversion was observed, which could be taken as proof of the absence of PTA leaching, at least during the period of time that the catalyst was evaluated. The test results are presented in Table 5.

**Table 5.** The results of hot filtration test for the PW4@MIL-100(Cr) catalyst.

Time (h)	Conversion (%)	
	(FAME:H <sub>2</sub> O <sub>2</sub> Molar Ratio of 1:2) *	(FAME:H <sub>2</sub> O <sub>2</sub> Molar Ratio of 1:8) *
0	0	0
1	36	49
after hot filtration		
2	37	50
3	38	51
4	37	52

\* Reaction conditions: FAME content of 1 wt%, temperature of 40 °C and catalyst content of 15 g·L<sup>-1</sup>.

The results of the PW4@MIL-100(Cr) catalyst recycling test are shown in Figure 8. The epoxidation reaction was carried out at 40 °C with a molar ratio of unsaturated FAMES:H<sub>2</sub>O<sub>2</sub> of 1:2 and a catalyst content of 15 g·L<sup>-1</sup> for 4 h.

The catalyst was separated through centrifugation, weighed and loaded into the reactor without any treatment after each reaction cycle. Then, the required amounts of FAMES and acetonitrile were loaded into the reactor, and the mixture was thermostated with stirring. The calculated amount of hydrogen peroxide was loaded into the reactor when the temperature reached 40 °C. After that, a sample of the reaction mixture was taken for analysis, and the beginning of the reaction was fixed.

As can be seen, the PW4@MIL-100(Cr) catalyst could be easily separated and reused without any treatment for five consecutive cycles without a significant loss of activity or selectivity (Figure 8).

After five catalytic cycles the PW4@MIL-100(Cr) catalyst was characterized through XRD, FTIR, BET, SEM and EDS.

The specific surface area and the pore volume were decreased (see Table 6), and some agglomeration of the catalyst powder was observed (see Supplementary Materials, Figure

S14) after five cycles, which indicated the reaction products' deposition on the catalyst surface. The results of the element analysis (Table 7) also confirmed this fact.

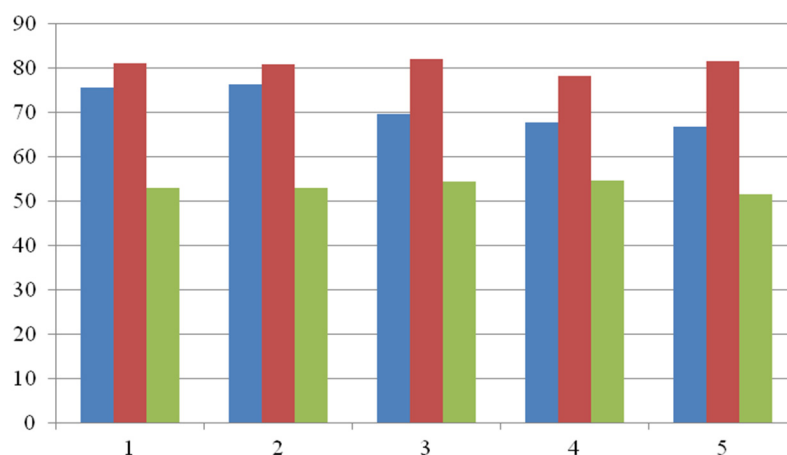


**Figure 8.** Reusability of catalyst. Reaction conditions: FAME content of 1 wt%; temperature of 40 °C; catalyst content of 15 g·L<sup>-1</sup>; unsaturated FAME:H<sub>2</sub>O<sub>2</sub> molar ratio of 1:2; reaction time of 4 h; blue—ester conversion, %; red—epoxide selectivity, %; and green—hydrogen peroxide conversion, %.

**Table 6.** Textural properties of fresh and spent PW4@MIL-100(Cr) catalysts.

Catalyst	BET Surface Areas, m <sup>2</sup> ·g <sup>-1</sup>	Pore Volume, cm <sup>3</sup> ·g <sup>-1</sup>
PW4@MIL-100(Cr) (fresh)	910 ± 26	0.5
PW4@MIL-100(Cr) (after 1 catalytic cycle)	583 ± 18	0.4
PW4@MIL-100(Cr) (after 5 catalytic cycles)	283 ± 7	0.3

**Table 7.** Catalyst EDS analysis results.

Catalyst	C (atomic%)	Cr (atomic%)	P (atomic%)	W (atomic%)	P/W/Cr
PW4@-MIL-100(Cr) (fresh)	54.21	4.98	0.46	2.13	1/4.6/10.8
PW4@-MIL-100(Cr) (after 1 catalytic cycle)	54.67	4.82	0.45	2.05	1/4.6/10.4
PW4@-MIL-100(Cr) (after 5 catalytic cycles)	57.57	4.70	0.43	1.95	1/4.5/10.2

As regards the MOF destruction, the XRD technique did not show significant changes in the PW4@-MIL-100(Cr) structure after five catalytic cycles (see Supplementary Materials, Figure S15). FTIR spectroscopy (see Supplementary Materials, Figure S16) also did not reveal significant changes. It should also be noted that, after the catalytic tests, the P/W/Cr ratio was retained, which confirmed the absence of framework destruction. Otherwise, when the framework was destroyed, PW4 leaching should have occurred and as a result of which the ratio should have changed.

### 3. Materials and Methods

#### 3.1. Materials

FAMES (content: methyl palmitate—5.1%, methyl oleate—59.4%, methyl linoleate—24.6%, methyl stearate—2.1%, methyl linolenate—7.9% and others—0.9%) were obtained through rapeseed oil transesterification with methanol as described previously [66].

Epoxidized FAMES (oxygen oxirane content value of 3.8 wt% and 90.0 wt%) used for the preparation of standard solutions were obtained through FAME epoxidation with hydrogen peroxide using performic acid. The epoxidation was carried out in a glass flask equipped with a mechanical stirrer, thermostatic jacket and reflux condenser. FAMES were

weighed and were charged in the reactor. Under continuous stirring, FAMES were acidified with formic acid and were heated. Then, hydrogen peroxide was slowly added dropwise. After the reaction was finished, reaction mixture was taken out and thoroughly washed with water to a neutral pH. Reaction conditions: FAME:HCOOH:H<sub>2</sub>O<sub>2</sub> molar ratio of 1:5:2, temperature of 45 °C and reaction time of 150 min.

Trimesic acid (95.0 wt%) and nonyl aldehyde (95.0 wt%) were obtained from Sigma–Aldrich (Saint Louis, MO, USA). Acetonitrile was obtained from Scharlau (Barcelona, Spain). Hydrofluoric acid (40.0 wt%), methyl alcohol (99.5 wt%), acetone (99.8 wt%), phosphotungstic acid hydrate (99.5 wt%), phosphoric acid (85.0 wt%), Cr(NO<sub>3</sub>)<sub>3</sub>·9H<sub>2</sub>O (99.0 wt%), acetic acid (99.5 wt%), potassium iodide (99.5 wt%), methyl ester 9-oxo-nonanoic acid (98 wt%), methyl 10-oxooctadecanoate (98.0 wt%) and hydrogen peroxide (35 wt%) were obtained from Vekton (St. Petersburg, Russia). Analytical standard methyl stearate (99.0 wt% purity) was obtained from Sigma–Aldrich.

Unless otherwise stated, all chemicals in this work were commercially available and used without further purification. Deionized water was used in all the experiments.

### 3.2. Catalyst Preparation

#### 3.2.1. Synthesis of MIL-100(Cr)

MIL-100(Cr) was obtained through the hydrothermal method as described previously [64]. Cr(NO<sub>3</sub>)<sub>3</sub>·9H<sub>2</sub>O (10 mmol), trimesic acid (10 mmol), aqueous solution of hydrofluoric acid (10 wt%, 10 mmol) and 50 mL of deionized water were placed in a Teflon-lined autoclave reactor with a volume of 100 mL. The resulting mixture was kept at 220 °C for 8 h. The resulting powder was previously washed with water to a neutral pH and then was washed with methanol and acetone. The washed catalyst was dried in a vacuum oven at 40 °C overnight.

#### 3.2.2. Synthesis of PW12@MIL-100(Cr)

PW12@MIL-100(Cr) was obtained through the hydrothermal method. Cr(NO<sub>3</sub>)<sub>3</sub>·9H<sub>2</sub>O (10 mmol), trimesic acid (10 mmol), aqueous solution of hydrofluoric acid (10 wt%, 10 mmol), phosphotungstic acid (1.4 mmol) and 50 mL of deionized water were placed into a Teflon-lined autoclave reactor with a volume of 100 mL. The resulting mixture was kept at 220 °C for 8 h. The resulting powder was previously washed with water to a neutral pH and then was washed with methanol and acetone. The washed catalyst was dried in a vacuum oven at 40 °C overnight.

#### 3.2.3. Synthesis of PW4@MIL-100(Cr)

PW4@MIL-100(Cr) was obtained by treating PW12@MIL-100(Cr) with hydrogen peroxide and phosphoric acid. PW12@MIL-100(Cr) (2 g), aqueous solution of hydrogen peroxide (30 wt%, 30 g) and aqueous solution of phosphoric acid (5 mol·L<sup>-1</sup>, 0.1 mL) were placed into a glass laboratory batch reactor equipped with a thermostatic jacket, magnetic stirrer and reflux condenser. The resulting slurry was stirred for 4 h at 40 °C. The resulting powder was washed with water and dried in a vacuum oven at 40 °C for 4 h.

### 3.3. Catalyst Characterization

X-ray diffraction (XRD) patterns were recorded with a Shimadzu XRD-6100 diffractometer (Shimadzu, Kyoto, Japan) using Cu K $\alpha$  radiation ( $\lambda = 0.1541$  nm) in the 2 $\theta$  range from 10° to 50° with a step size of 0.02°.

The elemental composition and morphology of the catalyst surface were determined on a JSM-7600F scanning electron microscope (JEOL, Tokyo, Japan) equipped with the energy dispersive analyzer INCA Energy TEM 250 X-Max.

The pore size and specific surface area of the obtained samples were measured using a Sorbi MS instrument (META, Novosibirsk, Russia). Sample preparation included dehydration for 2 h at 110 °C and preliminary thermal treatment at 100 °C. To obtain a complete

adsorption–desorption isotherm, the absolute calibration method was used. The specific surface area was measured using the BET method.

Raman spectra were recorded using a NTEGRA Spectra instrument (NTEGRA, Zenograd, Russia) equipped with laser line of 473 nm. Laser power was kept at 3.6 mW.

The KBr pellet technique was applied to determine IR specters of the catalyst samples. IR spectra were recorded in air at room temperature using Shimadzu IRAffinity–1 spectrometer (Shimadzu, Kyoto, Japan) in the region of wavenumbers from 400 to 4000  $\text{cm}^{-1}$  with a resolution of 0.5  $\text{cm}^{-1}$ .

The concentration of the Brønsted acid centers was determined through the back titration method using sodium chloride as an anion-exchange agent [67]. In a typical experiment, 100 mg of the sample was suspended in a saturated aqueous NaCl solution (10 mL). The resulting slurry was previously treated with ultrasound and was then stirred for 20 h and centrifuged. The separated powder was further washed with water (10 mL) for 20 min and was centrifuged. The resulting centrifugates were mixed and titrated with a NaOH solution (0.005  $\text{mol}\cdot\text{L}^{-1}$ ).

### 3.4. Catalytic Test Procedure

The FAME epoxidation was carried out in a glass laboratory batch reactor equipped with a thermostatic jacket, magnetic stirrer and reflux condenser. A calculated amount of FAMEs, hydrogen peroxide and solvent were placed into the reactor, and the mixture was heated with stirring (600 rpm). After reaching the desired temperature, a weighed sample of the catalyst was added to the mixture, and the beginning of the reaction was fixed. During the process, the reaction liquid samples were taken at predetermined time intervals. Each experiment was reproduced at least 2 times.

### 3.5. Analysis

Before analysis, the liquid samples were rapidly cooled to room temperature and centrifuged.

The product identifications and quantitative analyses were performed through GC-MS using a Shimadzu GC-2010 instrument equipped with a GCMS-QP2020 mass spectrometer, FID and VB-1701 capillary column (length of 30 m, inner diameter of 0.25 mm and film thickness of 0.25  $\mu\text{m}$ ; VICI, Poughkeepsie, NY, USA). The substrate and product concentrations were quantified using the calibration curves of methyl stearate and epoxidized FAME standard solutions in acetonitrile. Conversion, selectivity, and yield were determined with the following formulas:

$$\text{Conversion}_{\text{FAME}}(\%) = \frac{n_0(\text{FAME}) - n_i(\text{FAME})}{n_0(\text{FAME})} * 100 \quad (1)$$

$$\text{Conversion}_{\text{H}_2\text{O}_2}(\%) = \frac{n_0(\text{H}_2\text{O}_2) - n_i(\text{H}_2\text{O}_2)}{n_0(\text{H}_2\text{O}_2)} * 100 \quad (2)$$

$$\text{Selectivity}_{\text{EFAME}}(\%) = \frac{n_i(\text{EFAME})}{n_0(\text{FAME}) - n_i(\text{FAME})} * 100 \quad (3)$$

$$\text{Yield}_{\text{EFAME}}(\%) = \frac{X_{\text{FAME}} * S_{\text{EFAME}}}{100} \quad (4)$$

The oligomerization products were identified through HPLC-MS using Agilent 1200 HPLC system equipped with an Agilent 6310 mass detector and C18 column (250  $\times$  4.6 mm).

The concentration of hydrogen peroxide in the reaction mixture was determined using standard iodometric titration as described previously [68].

Standard deviation was  $\pm 2\%$  and  $\pm 3\%$  for conversion and selectivity values, respectively.

#### 4. Conclusions

The MIL-100(Cr), PW12@MIL-100(Cr) and PW4@MIL-100(Cr) were prepared, characterized through various methods (XRD, FT-IR, BET, SEM and EDS) and tested as catalysts in the epoxidation of unsaturated FAMES with hydrogen peroxide.

The peroxopolyoxotungstate PW4 encapsulated in the MIL-100(Cr) matrix showed a good catalytic activity and selectivity. The reaction using PW4@MIL-100(Cr) gave epoxides with a 77% selectivity and a 95% unsaturated FAME conversion in optimal conditions (reaction time of 4 h, temperature of 40 °C, FAME:H<sub>2</sub>O<sub>2</sub> molar ratio of 1:8 and catalyst loading of 15 g·L<sup>-1</sup>). At the same time, the PW12@MIL-100(Cr) sample was significantly less active and showed results similar to the MIL-100(Cr) results.

The PW4@MIL-100(Cr) catalyst exhibited a good stability and reusability for five consecutive reaction cycles without a significant loss of activity or selectivity.

**Supplementary Materials:** The following Supplementary Materials can be downloaded at <https://www.mdpi.com/article/10.3390/catal13010138/s1>, Figure S1: SEM images of (a,b) MIL-100(Cr); Figure S2: SEM images of (a,b) PW12@MIL-100(Cr); Figure S3: SEM images of (a,b) PW4@MIL-100(Cr); Figure S4: EDS analysis of PW12@MIL-100(Cr); Figure S5: EDS analysis of PW4@MIL-100(Cr); Figure S6: N<sub>2</sub> isotherm adsorption of MIL-100(Cr); Figure S7: N<sub>2</sub> isotherm adsorption of PW12@MIL-100(Cr); Figure S8: N<sub>2</sub> isotherm adsorption of PW4@MIL-100(Cr); Figure S9: N<sub>2</sub> isotherm adsorption of PW4@MIL-100(Cr) after 1 cycles; Figure S10: N<sub>2</sub> isotherm adsorption of PW4@MIL-100(Cr) after 5 cycles; Figure S11: Mass spectrum of FAME oxidation products (GC-MS). (a) methyl 5-oxo-octadecanoate, (b) Methyl 9-oxononanoate, (c) methyl 10-oxo-octadecanoate; Figure S12: Mass spectrum of FAME Oligomerization products (HPLC-MS). Mass spectrum (positive) of peaks with a retention time of 25.5 min; 25.9 min; 26.2 min; 26.9 min; 28.5 min; Figure S13: Mass spectrum of methyl stearate oxidation products (GC-MS). (a) methyl 5-oxo-octadecanoate, (b) methyl 10-oxo-octadecanoate, (c) methyl 17-oxo-octadecanoate; Figure S14: SEM images of (a) fresh PW4@MIL-100(Cr) and (b) spent PW4@MIL-100(Cr) powders; Figure S15: XRD patterns of PW4@MIL-100(Cr) fresh prepared (a) and after 5 catalytic cycle (b); and Figure S16: FTIR spectra of PW4@MIL-100(Cr) fresh prepared (a) and after 5 catalytic cycle (b).

**Author Contributions:** Conceptualization, A.L.E.; methodology, A.L.E. and E.A.K., validation, E.A.K. and T.A.C.; formal analysis, A.L.E. and K.V.O.; investigation, A.L.E., E.A.K., T.A.C. and K.V.O., resources, A.L.E. and K.V.O.; data curation, A.L.E. and E.A.K.; writing—original draft preparation, A.L.E., T.A.C. and E.A.K.; writing—review and editing, A.L.E., T.A.C. and E.A.K.; visualization, E.A.K., T.A.C. and K.V.O.; supervision, A.L.E.; project administration, A.L.E. and E.A.K. All authors have read and agreed to the published version of the manuscript.

**Funding:** The investigation was financially supported by the Ministry of Science and Higher Education of the Russian Federation as part of the scientific project the Laboratory of biofuels (BioFuelLab), project number FSWR-2022-0003.

**Data Availability Statement:** New data are contained within the article. Other data were cited and listed in the bibliography.

**Conflicts of Interest:** The authors declare no conflict of interest.

#### References

1. Mudiyansele, A.Y.; Yao, H.; Viamajala, S.; Varanasi, S.; Yamamoto, K. Efficient Production of Alkanolamides from Microalgae. *Ind. Eng. Chem. Res.* **2015**, *54*, 4060–4065. [\[CrossRef\]](#)
2. Fairweather, N.T.; Gibson, M.S.; Guan, H. Homogeneous Hydrogenation of Fatty Acid Methyl Esters and Natural Oils under Neat Conditions. *Organometallics* **2015**, *34*, 335–339. [\[CrossRef\]](#)
3. Tan, S.G.; Chow, W.S. Biobased Epoxidized Vegetable Oils and Its Greener Epoxy Blends: A Review. *Polym.-Plast. Technol. Eng.* **2010**, *49*, 1581–1590. [\[CrossRef\]](#)
4. Belousov, A.S.; Esipovich, A.L.; Kanakov, E.A.; Otopkova, K.V. Recent advances in sustainable production and catalytic transformations of fatty acid methyl esters. *Sustain. Energy Fuels* **2021**, *5*, 4512–4545. [\[CrossRef\]](#)
5. Liu, J.; Tao, B. Thermodynamically predicting liquid/solid phase change of long-chain fatty acid methyl esters (FAMES) and its application in evaluating the low-temperature performance of biodiesel. *J. Taiwan Inst. Chem. Eng.* **2022**, *135*, 104384. [\[CrossRef\]](#)
6. Xie, Q.; Zhu, H.; Xu, P.; Xing, K.; Yu, S.; Liang, X.; Ji, W.; Nie, Y.; Ji, J. Transesterification of methyl oleate for sustainable production of biolubricant: Process optimization and kinetic study. *Ind. Crops. Prod.* **2022**, *182*, 114879. [\[CrossRef\]](#)

7. Targhan, H.; Evans, P.; Bahrami, K. A review of the role of hydrogen peroxide in organic transformations. *J. Ind. Eng. Chem.* **2021**, *104*, 295–332. [[CrossRef](#)]
8. Rostamnia, S.; Gholipour, B.; Liu, X.; Wang, Y.; Arandiyan, H. NH<sub>2</sub>-coordinately immobilized tris(8-quinolinolato)iron onto the silica coated magnetite nanoparticle: Fe<sub>3</sub>O<sub>4</sub>@SiO<sub>2</sub>-FeQ<sub>3</sub> as a selective Fentonlike catalyst for clean oxidation of sulfides. *J. Colloid Interface Sci.* **2018**, *511*, 447–455. [[CrossRef](#)]
9. Rostamnia, S.; Mohsenzad, F. Nanoarchitecturing of open metal site Cr-MOFs for oxodiperoxo molybdenum complexes [MoO(O<sub>2</sub>)<sub>2</sub>@En/MIL-100(Cr)] as promising and bifunctional catalyst for selective thioether oxidation. *Mol. Catal.* **2018**, *445*, 12–20. [[CrossRef](#)]
10. Doustkhah, E.; Rostamnia, S.; Gholipour, B.; Zeynizadeh, B.; Baghban, A.; Luque, R. Design of chitosan-dithiocarbamate magnetically separable catalyticnanocomposites for greener aqueous oxidations at room temperature. *Mol. Catal.* **2017**, *434*, 7–15. [[CrossRef](#)]
11. Rostamnia, S.; Doustkhah, E.; Golchin-Hosseini, H.; Zeynizadeh, B.; Xin, H.; Luque, R. Efficient tandem aqueous room temperature oxidative amidations catalysed by supported Pd nanoparticles on graphene oxide. *Catal. Sci. Technol.* **2016**, *6*, 4124–4133. [[CrossRef](#)]
12. Rostamnia, S.; Alamgholiloo, H.; Jafari, M.; Rookhosh, R.; Abbasi, A.R. Synthesis and catalytic study of open metal site metal-organic frameworks of Cu<sub>3</sub>(BTC)<sub>2</sub> microbelts in selective organic sulfide oxidation. *Appl. Organometal. Chem.* **2016**, *30*, 954–958. [[CrossRef](#)]
13. Kholdeeva, O.A. Recent developments in liquid-phase selective oxidation using environmentally benign oxidants and mesoporous metal silicates. *Catal. Sci. Technol.* **2014**, *4*, 1869–1889. [[CrossRef](#)]
14. Khomane, R.B.; Kulkarni, B.D.; Paraskar, A.; Sainkar, S.R. Synthesis, characterization and catalytic performance of titanium silicalite-1 prepared in micellar media. *Mater. Chem. Phys.* **2002**, *76*, 99–103. [[CrossRef](#)]
15. Grieneisen, J.L.; Kessler, H.; Fache, E.; Le Govic, A.M. Synthesis of TS-1 in fluoride medium. A new way to a cheap and efficient catalyst for phenol hydroxylation. *Microporous Mesoporous Mater.* **2000**, *37*, 379–386. [[CrossRef](#)]
16. Xinhua, L.; Zhentao, M.; Yaquan, W.; Li, W.; Xiangwen, Z.; Wei, W.; Enze, M.; Songbao, F. Process integration of H<sub>2</sub>O<sub>2</sub> generation and the ammoximation of cyclohexanone. *J. Chem. Technol. Biotechnol.* **2004**, *79*, 658–662.
17. Halasz, I.; Agarwal, M.; Senderov, E.; Marcus, B. Efficient oxyfunctionalization of n-hexane by aqueous H<sub>2</sub>O<sub>2</sub> over a new TS-PQ<sup>TM</sup> catalyst. *Catal. Today* **2003**, *81*, 227–245. [[CrossRef](#)]
18. Gao, X.; Zhang, Y.; Hong, Y.; Luo, B.; Yan, X.; Wu, G. Efficient and clean epoxidation of methyl oleate to epoxidized methyl oleate catalyzed by external surface of TS-1 supported molybdenum catalysts. *Microporous Mesoporous Mater* **2022**, *333*, 111731. [[CrossRef](#)]
19. Liu, H.; Wang, Y.; Ye, T.; Wang, F.; Ran, S.; Xie, H.; Liu, J.; Li, Y.; Li, B.; Liu, Y.; et al. Fully utilizing seeds solution for solvent-free synthesized nanosized TS-1 zeolites with efficient epoxidation of chloropropene. *J. Solid State Chem.* **2022**, *307*, 122844. [[CrossRef](#)]
20. Wilde, N.; Pelz, M.; Gebhardt, S.G.; Gläser, R. Highly efficient nano-sized TS-1 with micro-/mesoporosity from desilication and recrystallization for the epoxidation of biodiesel with H<sub>2</sub>O<sub>2</sub>. *Green Chem.* **2015**, *17*, 3378–3389. [[CrossRef](#)]
21. Wilde, N.; Přeč, J.; Pelz, M.; Kubů, M.; Čejka, J.; Gläser, R. Accessibility enhancement of TS-1-based catalysts for improving the epoxidation of plant oil-derived substrates. *Catal. Sci. Technol.* **2016**, *6*, 7280–7288. [[CrossRef](#)]
22. Esipovich, A.L.; Belousov, A.S.; Kanakov, E.A.; Mironova VYu Rogozhin, A.E.; Danov, S.M.; Vorotyntsev, A.V.; Makarov, D.A. Solvent Effects in Epoxidation of Fatty Acid Methyl Esters with Hydrogen Peroxide over TS-1 Catalyst. *Kinet. Catal.* **2019**, *60*, 62–68. [[CrossRef](#)]
23. Wilde, N.; Worch, C.; Suprun, W.; Gläser, R. Epoxidation of biodiesel with hydrogen peroxide over Ti-containing silicate catalysts. *Microporous Mesoporous Mater.* **2012**, *164*, 182–189. [[CrossRef](#)]
24. Cambor, M.A.; Corma, A.; Esteve, P.; Martinez, A.; Valencia, S. Epoxidation of unsaturated fatty esters over large-pore Ti-containing molecular sieves as catalysts: Important role of the hydrophobic–hydrophilic properties of the molecular sieve. *Chem. Commun.* **1997**, *8*, 795–796. [[CrossRef](#)]
25. Guidotti, M.; Psaro, R.; Ravasio, N.; Sgobba, M.; Gianotti, E.; Grinberg, S. Titanium–Silica Catalysts for the Production of Fully Epoxidised Fatty Acid Methyl Esters. *Catal. Lett.* **2008**, *122*, 53–56. [[CrossRef](#)]
26. Rios, L.A.; Weckes, H.P.; Schuster, H.; Hoelderich, W.F. Mesoporous and amorphous Ti–silicas on the epoxidation of vegetable oils. *J. Catal.* **2005**, *232*, 19–26. [[CrossRef](#)]
27. Goyal, R.; Singh, O.; Agrawal, A.; Samanta, C.; Sarkar, B. Advantages and limitations of catalytic oxidation with hydrogen peroxide: From bulk chemicals to lab scale process. *Catal. Rev.* **2020**, *64*, 229–285. [[CrossRef](#)]
28. Yahya, R.; Craven, M.; Kozhevnikova, E.F.; Steiner, A.; Samunual, P.; Kozhevnikov, I.V.; Bergbreiter, D.E. Polyisobutylene oligomer-bound polyoxometalates as efficient and recyclable catalysts for biphasic oxidations with hydrogen peroxide. *Catal. Sci. Technol.* **2015**, *5*, 818–821. [[CrossRef](#)]
29. Omwoma, S.; Gore, C.T.; Ji, Y.; Hu, C.; Song, Y.-F. Environmentally benign polyoxometalate materials. *Coord. Chem. Rev.* **2015**, *286*, 17–29. [[CrossRef](#)]
30. Venturello, C.; D’Aloisio, R.; Bart, J.C.J.; Ricci, M. A New peroxotungsten heteropoly anion with special oxidizing properties: Synthesis and structure of tetrahexylammonium tetra(diperoxotungsto)phosphate(3-). *J. Mol. Catal.* **1985**, *32*, 107–110. [[CrossRef](#)]

31. Ishii, Y.; Yamawaki, K.; Ura, T.; Yamada, H.; Yoshida, T.; Ogawa, M. Hydrogen peroxide oxidation catalyzed by heteropoly acids combined with cetylpyridinium chloride. Epoxidation of olefins and allylic alcohols, ketonization of alcohols and diols, and oxidative cleavage of 1,2-diols and olefins. *J. Org. Chem.* **1988**, *53*, 3587–3593. [[CrossRef](#)]
32. Poli, E.; Clacens, J.-M.; Barrault, J.; Pouilloux, Y. Solvent-free selective epoxidation of fatty esters over a tungsten-based catalyst. *Catal. Today* **2009**, *140*, 19–22. [[CrossRef](#)]
33. Craven, M.; Xiao, D.; Kunstmann-Olsen, C.; Kozhevnikova, E.F.; Blanc, F.; Steiner, A.; Kozhevnikov, I.V. Oxidative desulfurization of diesel fuel catalyzed by polyoxometalate immobilized on phosphazene-functionalized silica. *Appl. Catal. B* **2018**, *231*, 82–91. [[CrossRef](#)]
34. Poli, E.; De Sousa, R.; Jérôme, F.; Pouilloux, Y.; Clacens, J.M. Catalytic epoxidation of styrene and methyl oleate over peroxophotungstate entrapped in mesoporous SBA-15. *Catal. Sci. Technol.* **2012**, *2*, 910–914. [[CrossRef](#)]
35. Hoegaerts, D.; Sels, B.F.; De Vos, D.E.; Verpoort, F.; Jacobs, P.A. Heterogeneous tungsten-based catalysts for the epoxidation of bulky olefins. *Catal. Today* **2000**, *60*, 209–218. [[CrossRef](#)]
36. De Villa, P.A.L.; Sels, B.F.; De Vos, D.E.; Jacobs, P.A. A Heterogeneous Tungsten Catalyst for Epoxidation of Terpenes and Tungsten-Catalyzed Synthesis of Acid-Sensitive Terpene Epoxides. *J. Org. Chem.* **1999**, *64*, 7267–7270. [[CrossRef](#)]
37. Poli, E.; Clacens, J.M.; Pouilloux, Y. Synthesis of peroxophotungstate immobilized onto polymeric support as heterogeneous catalyst for the epoxidation of unsaturated fatty esters. *Catal. Today* **2011**, *164*, 429–435. [[CrossRef](#)]
38. Gándara, F.; Andrés, A.; Gómez-Lor, B.; Gutiérrez-Puebla, E.; Iglesias, M.; Monge, M.A.; Proserpio, D.M.; Snejko, N. A Rare-Earth MOF Series: Fascinating Structure, Efficient Light Emitters, and Promising Catalysts. *Cryst. Growth Des.* **2008**, *8*, 378–380. [[CrossRef](#)]
39. Hu, M.; Safarifard, V.; Doustkhah, E.; Rostamnia, S.; Morsali, A.; Nouruzi, N.; Beheshti, S.; Akhbari, K. Taking organic reactions over metal-organic frameworks as heterogeneous catalysis. *Microporous Mesoporous Mater.* **2018**, *256*, 111–127. [[CrossRef](#)]
40. Alamgholiloo, H.; Rostamnia, S.; Zhang, K.; Lee, T.H.; Lee, Y.; Varma, R.S.; Jang, H.W.; Shokouhimehr, M. Boosting Aerobic Oxidation of Alcohols via Synergistic Effect between TEMPO and a Composite Fe<sub>3</sub>O<sub>4</sub>/Cu-BDC/GO Nanocatalyst. *ACS Omega* **2020**, *5*, 5182–5191. [[CrossRef](#)]
41. Babaee, S.; Zarei, M.; Sepehrmansourie, H.; Zolfigol, M.A.; Rostamnia, S. Synthesis of Metal–Organic Frameworks MIL-101(Cr)-NH<sub>2</sub> Containing Phosphorous Acid Functional Groups: Application for the Synthesis of N-Amino-2-pyridone and Pyrano [2,3-c]pyrazole Derivatives via a Cooperative Vinylogous Anomeric-Based Oxidation. *ACS Omega* **2020**, *5*, 6240–6249. [[CrossRef](#)]
42. Alamgholiloo, H.; Rostamnia, S.; Hassankhani, A.; Liu, X.; Eftekhari, A.; Hasanzadeh, A.; Zhang, K.; Karimi-Maleh, H.; Khaksar, S.; Varma, R.S.; et al. Formation and stabilization of colloidal ultra-small palladium nanoparticles on diamine-modified Cr-MIL-101: Synergic boost to hydrogen production from formic acid. *J. Colloid Interface Sci.* **2020**, *567*, 126–135. [[CrossRef](#)]
43. Kim, M.; Cahill, J.F.; Fei, H.; Prather, K.A.; Cohen, S.M. Postsynthetic Ligand and Cation Exchange in Robust Metal–Organic Frameworks. *J. Am. Chem. Soc.* **2012**, *134*, 18082–18088. [[CrossRef](#)]
44. Sua, S.; Lia, X.; Zhanga, X.; Zhuh, J.; Liua, G.; Tana, M.; Wang, Y.; Luoa, M. Keggin-type SiW<sub>12</sub> encapsulated in MIL-101(Cr) as efficient heterogeneous photocatalysts for nitrogen fixation reaction. *J. Colloid Interface Sci.* **2022**, *621*, 406–415. [[CrossRef](#)]
45. Abbasia, F.; Karimi-Sabetb, J.; Abbasia, Z.; Ghotbia, C. Improved method for increasing accessible pores of MIL-101(Cr) by encapsulation and removal of Phosphotungstic acid (PTA): Pd/PTA-MIL-101(Cr) as an effective catalyst for CO oxidation. *J. Clean. Prod.* **2022**, *347*, 131168. [[CrossRef](#)]
46. Maksimchuk, N.V.; Kovalenko, K.A.; Arzumanov, S.S.; Chesalov, Y.A.; Melgunov, M.S.; Stepanov, A.G.; Fedin, V.P.; Kholdeeva, O.A. Hybrid Polyoxotungstate/MIL-101 Materials: Synthesis, Characterization, and Catalysis of H<sub>2</sub>O<sub>2</sub>-Based Alkene Epoxidation. *Inorg. Chem.* **2010**, *49*, 2920–2930. [[CrossRef](#)]
47. Wang, X.; Li, L.; Liang, J.; Huang, Y.; Cao, R. Boosting Oxidative Desulfurization of Model and Real Gasoline over Phosphotungstic Acid Encapsulated in Metal–Organic Frameworks: The Window Size Matters. *ChemCatChem* **2016**, *9*, 971–979. [[CrossRef](#)]
48. Jinzhu, C.; Shengpei, W.; Jing, H.; Limin, C.; Longlong, M.; Xing, H. Conversion of Cellulose and Cellobiose into Sorbitol Catalyzed by Ruthenium Supported on a Polyoxometalate/Metal–Organic Framework Hybrid. *ChemSusChem* **2013**, *6*, 1545–1555.
49. Meng, C.; Jiaqi, Y.; Ying, T.; Yongfei, L.; Zhimin, W.; Langsheng, P.; Yuejin, L. Hydroxyalkylation of Phenol with Formaldehyde to Bisphenol F Catalyzed by Keggin Phosphotungstic Acid Encapsulated in Metal–Organic Frameworks MIL-100(Fe or Cr) and MIL-101(Fe or Cr). *Ind. Eng. Chem. Res.* **2015**, *54*, 11804–11813.
50. Wang, D.; Ke, Y.; Guo, D.; Guo, H.; Chen, J.; Weng, W. Facile fabrication of cauliflower-like MIL-100(Cr) and its simultaneous determination of Cd<sup>2+</sup>, Pb<sup>2+</sup>, Cu<sup>2+</sup> and Hg<sup>2+</sup> from aqueous solution. *Sens. Actuators B* **2015**, *216*, 504–510. [[CrossRef](#)]
51. Ferey, G.; Serre, C.; Mellot-Draznieks, C.; Millange, F.; Surble, S.; Dutour, J.; Margiolaki, I. A hybrid solid with giant pores prepared by a combination of targeted chemistry, simulation, and powder diffraction. *Angew. Chem. Int. Ed.* **2004**, *43*, 6296–6301. [[CrossRef](#)] [[PubMed](#)]
52. Momma, K.; Izumi, F. VESTA 3 for three-dimensional visualization of crystal, volumetric and morphology data. *J. Appl. Crystallogr.* **2011**, *44*, 1272–1276. [[CrossRef](#)]
53. Panpan, M.; Gang, L.; Guoquan, Z.; Hong, L. Co(II)-salen complex encapsulated into MIL-100(Cr) for electrocatalytic reduction of oxygen. *J. Energy Chem.* **2014**, *23*, 507–512.
54. Siddiqui, S.; Khan, M.U.; Siddiqui, Z.N. Synthesis, Characterization, and Application of Silica-Supported Copper-Doped Phosphotungstic Acid in Claisen–Schmidt Condensation. *ACS Sustainable Chem. Eng.* **2017**, *5*, 7932–7941. [[CrossRef](#)]

55. Peipei, L.; Huawei, W.; Qiang, Z.; Yingxia, W.; Jinxiang, D.; Jinping, L. Solvent effect on the synthesis of MIL-96(Cr) and MIL-100(Cr). *Microporous Mesoporous Mater.* **2011**, *142*, 489–493.
56. Trolliet, C.; Coudurier, G.; Védrine, J.C. Influence of the nature and porosity of different supports on the acidic and catalytic properties of H<sub>3</sub>PW<sub>12</sub>O<sub>40</sub>. *Top. Catal.* **2001**, *15*, 73–81. [[CrossRef](#)]
57. Lv, H.; Zhao, H.; Cao, T.; Qian, L.; Wang, Y.; Zhao, G. Efficient degradation of high concentration azo-dye wastewater by heterogeneous Fenton process with iron-based metal-organic framework. *J. Mol. Catal. A Chem.* **2015**, *400*, 81–89. [[CrossRef](#)]
58. Lohe, M.R.; Rose, M.; Kaskel, S. Metal-organic framework (MOF) aerogels with high micro- and macroporosity. *Chem. Commun.* **2009**, *40*, 6056–6058. [[CrossRef](#)]
59. George, L.; Shakeela, K.; Rao, G.R.; Jaiswal, M. Probing the electric double-layer capacitance in Keggin-type polyoxometalate ionic liquid gated graphene transistor. *Phys. Chem. Chem. Phys.* **2018**, *20*, 18474–18483. [[CrossRef](#)]
60. Aubry, C.; Chottard, G.; Platzner, N.; Brégeault, J.-M.; Thouvenot, R.; Chauveau, C.; Huet, C.; Ledon, H. Reinvestigation of Epoxidation Using Tungsten-Based Precursors and Hydrogen Peroxide in a Biphasic Medium. *Inorg. Chem.* **1991**, *30*, 4409–4415. [[CrossRef](#)]
61. Hwang, Y.K.; Hong, D.-Y.; Chang, J.-S.; Seo, H.; Yoon, M.; Kim, J.; Jhung, S.H.; Serre, C.; Férey, G. Selective sulfoxidation of aryl sulfides by coordinatively unsaturated metal centers in chromium carboxylate MIL-101. *Appl. Catal. A* **2009**, *358*, 249–253. [[CrossRef](#)]
62. Maksimchuk, N.V.; Kovalenko, K.A.; Fedin, V.P.; Kholdeeva, O.A. Cyclohexane selective oxidation over metal-organic frameworks of MIL-101 family: Superior catalytic activity and selectivity. *Chem. Commun.* **2012**, *48*, 6812–6814. [[CrossRef](#)] [[PubMed](#)]
63. Kholdeeva, O.A.; Skobelev, I.Y.; Ivanchikova, I.D.; Kovalenko, K.A.; Fedin, V.P.; Sorokin, A.B. Hydrocarbon oxidation over Fe- and Cr-containing metal-organic frameworks MIL-100 and MIL-101— a comparative study. *Catal. Today* **2014**, *238*, 54–61. [[CrossRef](#)]
64. Vimont, A.; Goupil, J.-M.; Lavalley, J.-C.; Daturi, M.; Surblé, S.; Serre, C.; Millange, F.; Férey, G.; Audebrand, N. Investigation of Acid Sites in a Zeotypic Giant Pores Chromium(III) Carboxylate. *J. Am. Chem. Soc.* **2006**, *128*, 3218–3227. [[CrossRef](#)] [[PubMed](#)]
65. Arends, I.W.C.E.; Sheldon, R.A. Activities and stabilities of heterogeneous catalysts in selective liquid phase oxidations: Recent developments. *Appl. Catal. A* **2001**, *212*, 175–187. [[CrossRef](#)]
66. Esipovich, A.L.; Rogozhin, A.E.; Belousov, A.S.; Kanakov, E.A.; Danov, S.M. A comparative study of the separation stage of rapeseed oil transesterification products obtained using various catalysts. *Fuel Process. Technol.* **2018**, *173*, 153–164. [[CrossRef](#)]
67. Herbst, A.; Janiak, C. Selective glucose conversion to 5-hydroxymethylfurfural (5-HMF) instead of levulinic acid with MIL-101Cr MOF-derivatives. *N. J. Chem.* **2016**, *40*, 7958–7967. [[CrossRef](#)]
68. Fedosov, A.; Fedosova, M.; Postnikova, I.; Orekhov, S.; Gushchin, A.; Ryabinin, D.; Chuzhaykin, I. Synthesis and characterization of hierarchical titanium-containing silicas using different size templates. *J. Chem. Sci.* **2019**, *131*, 77. [[CrossRef](#)]

**Disclaimer/Publisher’s Note:** The statements, opinions and data contained in all publications are solely those of the individual author(s) and contributor(s) and not of MDPI and/or the editor(s). MDPI and/or the editor(s) disclaim responsibility for any injury to people or property resulting from any ideas, methods, instructions or products referred to in the content.